Made available by Hasselt University Library in https://documentserver.uhasselt.be

Impacts of load distribution and lane width on pavement rutting performance for automated vehicles

Peer-reviewed author version

YEGANEH, Ali; VANDOREN, Bram & PIRDAVANI, Ali (2021) Impacts of load distribution and lane width on pavement rutting performance for automated vehicles. In: International Journal of Pavement Engineering, 23 (12) , p. 4125-4135.

DOI: 10.1080/10298436.2021.1935938
Handle: http://hdl.handle.net/1942/34259

Impacts of Load Distribution and Lane Width on Pavement Rutting Performance for Automated Vehicles

Journal:	*International Journal of Pavement Engineering*
Manuscript ID	GPAV-2020-0564.R2
Manuscript Type:	Research Article
Keywords:	Automated vehicle, Pavement rutting performance, finite element, wander distribution, lane width

SCHOLARONE™
Manuscripts

Impacts of Load Distribution and Lane Width on Pavement Rutting Performance for Automated Vehicles

Abstract

With ongoing improvements in technical possibilities and the availability of faster computers and communication systems, considerable attention has been drawn to smart driving technologies and particularly to automated vehicles (AVs). The deployment of AVs would provide the opportunity to have more control over the dynamics of the vehicle, including its lateral movement, which can affect the pavement's long-term rutting performance. The controlled lateral movement of the AVs may also imply a reduced lane width. This paper evaluates the impacts of dedicating a reduced lane width to automated vehicles on pavement rutting performance, considering two lateral movement modes for AVs; zero-wander and uniform-wander distribution. A finite element model was developed using ABAQUS software based on the Indiana Department of Transportation/Purdue University accelerated pavement tester (APT) facility. The rutting simulation results of this study showed that the abrupt changes in the loading schemes of the zero- and uniform-wander modes (i.e., change of the loading time from zero to its maximum value) cause considerable accumulated rutting in the edges of the loading areas. This is significantly greater than the total rutting induced by the human-driven vehicles (HDVs) following the normal-wander mode, which causes a compensated rutting behaviour by a gradual increase in loading time. In other words, the maximum rutting depths occur at different locations along the transverse direction of the road for different loading distributions. Furthermore, the comparison between rutting depths in different lane widths reveals that when dedicating the narrower lane widths for AVs with a uniform-wander distribution, the pavement's total rutting depth would remarkably increase compared to the wider lanes.

Keywords: automated vehicle; pavement rutting performance; wander effect; finite element model; lane width

Word count: 7353 words

For Peer Review Only

Introduction

Over the past few years, automated vehicles have received considerable attention around the world. Automated driving may become a reality in the following decades because of its potential benefits, including reduced energy consumption, pollution, driver stress, and the cost of congestion, as well as increasing highway capacity, safety, green mobility, and the feasibility of alternative fuel vehicles and improving transport accessibility (Fagnant and Kockelman, 2015; Litman, 2015; Charles and Cas, 2017; Vahidi and Sciarretta, 2018).

The deployment of AV technologies has the potential to change the transportation sector on a global scale. The current transportation infrastructure is designed primarily for HDVs. Since vehicle-related technologies are advancing faster than ever, it is essential to better understand how and when conventional infrastructures may be affected by AVs' deployment. The transition of road infrastructures from HDVs to infrastructures that are appropriate for AVs implies an evolution in road design (Dennis *et al.*, 2017).

The literature shows that anything directly related to the road such as the road markings, road signage, lane width, barriers, road surface, pavements, speed bumps, curbs, parking areas, cycle paths, drainage systems, culverts, channels, and gullies might be affected by AVs' deployment (Kockelman *et al.*, 2016; Dennis *et al.*, 2017; Johnson, 2017). From the road infrastructure point of view, one of the crucial aspects of AVs' deployment is its impact on road pavement rutting performance. Rutting is the load-induced permanent deformation of a flexible pavement (White *et al.*, 2002). There are two types of pavement rutting: uplift rutting and compressive rutting (Hua and White, 2002). Compressive rutting is defined where the deformed surface is positioned under the original surface. Uplift rutting is defined by the uplifting of the roads' surface above the original surface. Figure 1 shows the two potential types of rutting surface profiles that may be observed after load application and the corresponding compressive, uplift, and

For Peer Review Only

total rutting depths. In type 1, the uplift rutting is observed outside of the wheel path. In this case, the total rutting depth can be calculated by the summation of the compressive and the uplift rutting. In type 2, the uplift rutting is also observed between the dual tyres in addition to outside of the wheel path. In this case, the total rutting depth is the distance in the vertical direction between the lowest point and its corresponding point on the string-line (i.e., a wire along the transverse direction from one edge of the lane to the other) (Hua and White, 2002).

Since the AVs' automatic steering control is expected to be more accurate than HDVs' manual control, it can give the designers the option to control the AVs' lateral position in the lane much more precisely than the one in HDVs. Accordingly, induced pavement damage from AVs loading depends on the AVs' lateral wandering patterns (Chen, Balieu and Kringos, 2016; Noorvand and Underwood, 2017; Chen *et al.*, 2019; Zhou *et al.*, 2019). There have been limited systematic studies on wheel wander performance of AVs so far. Chen et al. (2016) investigated AVs deployment's potential influences on the pavement's long-term rutting performance by means of finite element modelling on a large scale. They indicated that AVs' automatic steering control system could reduce the wheel wander distance and, thus, the repeated single point load caused by lane centring and keeping the wheel wander confined may accelerate the rutting damage. In other words, results extracted from finite element models of their study showed that if a highly accurate steering control is achieved using AVs in the future, it may accelerate the pavement rutting damage significantly compared to conventional vehicles. In another study, Chen et al. (2019) proposed four possible lateral control modes for managing automated trucks' lateral distribution: zero-wander mode, uniform-wander mode, double peak Gaussian mode, and two-section uniform mode. Based on their study's simulation results, it has been confirmed that automated trucks could be highly beneficial to the asphalt pavement performance due to the wider range of pavement being

For Peer Review Only

used with appropriate control of lateral movements. Focusing on the implication of truck positioning on pavement performance and design, Noorvand and Underwood (2017) conducted a study to consider the uniform and zero wheel wander modes in the Mechanistic-Empirical Pavement Design Guide (MEPDG) (McCullah and Gray, 2005) and compared them to the normal distribution wander mode. They showed that a uniform distribution would allow the vehicles to use a wide range of lane space and, thus, increases pavement performance. Zhou et al. (2019) considered a normal distribution for AVs with three times smaller wander distances and analysed the influences of AVs on pavement rutting life with the Texas Mechanistic-Empirical Flexible Pavement Design system. They indicated that the narrower wandering of AVs increases the pavement rutting depth by 30% when compared to HDVs lateral wandering. To optimize the lateral wandering of AVs, they proposed the uniform lateral wandering mode, which would prolong the pavement life. Gungor and Al-Qadi (2020) conducted a study to optimize AVs' platooning impacts on pavement life-cycle cost (LCC). By optimizing the lateral wandering of each group of platoons, they proposed a control strategy for AVs so as to decelerate pavement damage and increase pavement service life. With the application of the proposed control strategy on a case study, they showed that the total pavement LCC reduced by approximately 50% when compared to the AVs' channelized traffic (i.e., zero-wander).

One of the significant parameters that can influence the lateral wandering of vehicles is the traffic lane width. However, the effects of lane width on the AVs' lateral wandering and, consequently, pavement rutting performance have not been studied yet. Although a narrower lane can save space and reduce road construction and maintenance costs, its impact on pavement performance remains to be investigated. Therefore, in this paper, we will investigate the impacts

For Peer Review Only

of lane width combined with different wander distributions on pavement long-term rutting performance.

[Figure 1 near here]

Methodology

In this study, two-dimensional finite element (FE) models were considered to simulate the in-service pavement rutting performance considering different lane widths for AVs and HDVs. In this paper, only trucks are considered in the analysis because the pavement design depends primarily on truck traffic. Therefore, the acronym AVs only denotes the automated trucks in this paper. A finite element model was developed and validated based on the Indiana Department of Transportation/Purdue University accelerated pavement tester (APT) facility. The tyre loading was simulated in the pavements transverse direction to study the effects of AVs' wander distribution on pavement rutting performance. Different evaluation scenarios with different lane widths were assumed to assess the lane width effect on the wander distribution of AVs and HDVs. The following sections describe the finite element modelling, wheel wander simulating, and evaluation scenarios.

Finite Element Modelling

Previous studies have proven that FE modelling is a powerful method to model pavement long-term rutting performance (Huang, 1995; Hua, 1998; Hua and White, 2002; White *et al.*, 2002). In this study, we followed the FE modelling approach and utilized the commercial software ABAQUS (2009) to conduct the required simulations. The model geometry and finite element type used in this study, the material model, the tyre contact area and loading model, and the model validation are presented in the following sub-sections.

For Peer Review Only

Model Geometry and Finite Element Type

To create a base FE model that can be calibrated and validated to be used in this study, we developed a model using the characteristics of the Indiana Department of Transportation/Purdue University accelerated pavement tester (APT) facility, which has been utilized in several studies around hot mix asphalt (HMA) rutting performance (Huang, 1995; Hua, 1998; Hua and White, 2002). This APT facility test pit is 6.1 m (20 ft.) wide by 6.1 m (20 ft.) long and 1.8 m (6 ft.) deep. The pavement structure built in the test pit includes a 0.076 m (3 in) asphalt overlay on top of a 0.31 m (12 in) reinforced concrete slab and a 1.4 m (57 in) of pea gravel, which acts as a rigid foundation. The test pit walls are reinforced concrete.

Hua et al. (1998) compared responses from 3D and 2D models of the APT facility's test lane. The reported difference in predicted maximum rutting depths is less than 2%, which is not significant. Therefore, the 2D model is used in subsequent analyses in this study to save computational time. Hua et al. (1998) showed that both vertical and horizontal permanent deformations were uniform through the central portion of the APT test lane. For this reason, we used a plane-strain model in which we utilized the structured meshing technique using CPE4 elements. The model has six element layers in the vertical direction. The mesh size in the transverse direction is selected to match the tyre print's dimensions and configuration. The bottom boundary is assumed fixed, which means that nodes cannot move horizontally or vertically. The boundary nodes along the pavement edges are horizontally constrained but are free to move in the vertical direction.

Material Model

Asphalt mixture is a time, temperature, and stress-dependent material and is subjected to repeated loading causing elastic, plastic, visco-elastic, and visco-plastic responses (Perl, Uzan and

For Peer Review Only

Sides, 1983). The plastic material properties contribute to the permanent deformation of flexible pavements, characterized by a creep model that includes a time-dependent accumulation of strains produced by repeated traffic loads. Typical nonlinear creep behaviour can be divided into primary, secondary, and tertiary stages. With the application of load, the creep strain rate usually decays during the primary stage, and it remains constant at the secondary stage. Creep fracture may occur at the end of the tertiary zone (Hua, 1998). A standard creep model for modelling the primary and secondary creep stages of material deformation is the time-hardening creep model (also known as the power-law creep model), which has been used and validated frequently to simulate the rutting deformations in asphalt layers (Huang, 1995; Hua, 1998; Hua and White, 2002; Fang *et al.*, 2007; Al-Qadi *et al.*, 2009). Through this model, the wheel-wandering effects can also be considered simply by simulating the tyre loading time distribution in the pavement's transverse direction, confirmed by Hua et al. (1998). The nonlinear time-hardening creep model can determine the accumulation of creep strain (i.e., permanent deformation or rutting) and can be characterized by the effective stress, the equivalent uniaxial creep strain rate, and time as shown in Eq. (1):

$$\varepsilon^{cr} = A \times \sigma^{m} \times t^{n} \tag{1}$$

Where ε^{cr} is creep strain, σ is stress ($^{N}/_{m^2}$), t is loading time (s), and A, m, and n are material constants.

The material constants in the nonlinear time-hardening creep equation can be fitted using creep test data under various magnitudes of constant loads, while in this study, they were chosen directly from the literature (Hua and White, 2002). The selected value for parameter A and the constants m and n are $8.5 \times (10)^{-8}$, -7.5, and 0.8, respectively. The Young's modulus of

For Peer Review Only

3103 MPa and the Poisson's ratio of 0.3 were chosen for elastic material properties based on the APT facility mentioned above. However, the elastic material properties do not contribute to the permanent deformation of the layers.

Tyre Contact Area and Loading Model

This model is subjected to the loading of a single axle with dual tyres. The distance between the centres of the dual tyres was 0.335 m (13.2 in). The contact area between the tyre and pavement surface was assumed to be rectangular with a length of 0.1981 m (7.8 in) and a width of 0.1930 m (7.6 in). Tyre contact pressure is determined according to the APT facility and is assumed to be 523312 Pa (75.9 psi) uniformly distributed over the contact area. The wheel's speed in the APT is 2.22 m/s (8 km/h or 87.4891 in/s). Therefore, one pass loading time is 0.089 seconds, which is derived by dividing the tyre print's length by the wheel speed (0.198/2.22 = 0.089 s). The total loading time is the accumulated repetitions of the single load, so the total loading time for 5,000 passes is 445.77 seconds.

Model Validation

To verify the selected geometry, boundary conditions, element type, and meshing in the model and to validate the accuracy of the predicted maximum rutting depth, we conducted a comparison of the FE modelling and the APT result. Table 1 shows maximum compressive and uplift rutting depths of our FE model and the APT for 5000 passes. The results are very close, indicating that the FE model is reliable to be used in further analysis.

[Table 1 near here]

For Peer Review Only

In-Service Pavement Rutting Performance

The in-service pavement rutting depth accumulates over time with the application of repeated loads. Since this study's focus is on the rutting of the asphalt layer only, a single asphalt layer can be assumed as a pavement structure to predict in-service pavement rutting. Hence, we used the abovementioned validated model with the same model geometry, material properties, tyre pressure, and tyre contact area to predict the in-service pavement rutting. Considering the traffic data used in Zhou et al. (2019), we assumed that the pavement structure would carry 30 million standard equivalent 80-KN single axle loads within a 20-year design period at a speed of 90 km/h. By dividing the tyre print's length by the wheel speed, the loading time of one pass is 0.0079 seconds, so the total loading time for 30 million passes is 237720 seconds. It is worth noting that the primary purpose of this study is to provide quantitative comparisons of rutting depth values obtained from different simplified assumptions on the FE models. Accordingly, the assumed modelling conditions are hypothetical situations, and if we have the actual information about truck traffic, we can adapt these measures in the future. The other factor involved in the in-service rutting analysis is the lateral wheel wandering, which is discussed in the following section.

Wheel Wander Simulating

From a pavement performance point of view, the most considerable difference between AVs and HDVs is the vehicles' lateral wandering. In other words, for AVs, one could propose and develop a computer program to design appropriate algorithms for the AVs' lateral movements within the lane, based on theoretical calculations. However, this could not be true for HDVs because they are not programmable but controlled by humans, and their lateral movement pattern depends on several factors such as driver behaviour, environment, and road characteristics. Thus, HDVs' lateral movements may not be determined based on theoretical calculations, and it is not

For Peer Review Only

reliable to assume their lateral movements are confined to a certain predefined range. Accordingly, the objective of this study was to consider a reliable and representative lateral movement pattern for HDVs on the one hand and consider the potential lateral movement patterns for AVs suggested by previous studies (e.g., zero- and uniform-wander modes) on the other hand, to provide a quantitative comparison between their rutting performance, and present the AVs deployment effects in terms of pavement rutting performance for the different lane widths. For this purpose and for all analyses and comparisons, we kept all factors the same, except for the wheel wander and lane width. In the following sections, wheel wander for HDVs and AVs are discussed.

The Lateral Wheel Wander of Human-Driven Vehicles

For HDVs, Buiter et al. (1989) divided the factors that influence the lateral wandering of vehicles into the following categories:

- time (hour, day, and month);
- the heavy-goods vehicle used (type, load, and width);
- traffic conditions (speed, intensity, proportion of heavy goods vehicles, oncoming traffic, traffic restrictions, and visibility);
- road characteristics (the type of road, road surface, number of lanes, road roughness, traffic-lane width, the width of the hard shoulder, superelevation, alignment, and road markings); and
- environment (open area, woodlands, built-up area, flyovers, tunnels, traffic barriers, and obstacles).

Between these influential factors on drivers' lateral movement behaviour, there exist a lot of complex interactions. It is not possible to quantify all these parameters to calculate vehicles' wander distances. Several techniques have been used to measure the lateral wandering of vehicles

For Peer Review Only

(Benekohal, Hall and Miller Harlan w, 1958; Lee and Shankar, 1983; Buiter *et al.*, 1989; Blab and Litzjw, 1995; Timm and Priest, 2005; Erlingsson, Said and McGarvey, 2012). These studies generally concluded that the traffic lane's width is the most significant parameter in determining the wheel wander distance. They observed that the wider the lanes, the greater the lateral distribution of vehicles, or the fewer the number of loads over a specific point of the pavement's surface.

Very few studies identified the standard deviations of the wheel wander distribution for different lane widths. However, some field studies showed that generally, wheel wander tends to be normally distributed with a standard deviation (σ) ranging from 0.2 to 0.61 m (Buiter *et al.*, 1989; Erlingsson, 2004; Timm and Priest, 2005). The Highway Capacity Manual (HCM) (*2010*) specifies a range of lane widths from 3 m to 3.6 m, although it is possible to find lanes narrower than 3 m or wider than 3.6 m. Lateral wander distance values suggested in the MEPDG (McCullah and Gray, 2005) are 0.305 m, 0.254 m, and 0.203 m for lane widths greater than 3.6 meters, lane widths between 3 and 3.6 meters and lane widths less than 3 meters, respectively. However, the MEPDG (McCullah and Gray, 2005) does not have a detailed classification in the lane width ranging from 3 to 3.6 m.

Buiter et al. (1989) conducted an original and important fieldwork to identify the standard deviation (σ) of the wheel wander distributions for different lane widths. They obtained relevant field data from tests conducted with a specially developed measuring system, and they determined the standard deviation (also called the lateral spread or wander distance) associated with the normal distribution of vehicles across the traffic lane. By dividing the traffic lanes into three width classes, they determined the lateral spreads for each class. Based on Buiter et al. (1989) findings, we

For Peer Review Only

assumed the lane widths of 3.5, 3.25, and 3 m with a respective standard deviation (σ) of 0.29, 0.26, and 0.24 m in our study.

We calculated the transverse loading time distribution for one dual tyre for 30 million loading cycles (total loading time of 237720 seconds) for each lane width (see Figure 2). We used the superposition method used in Hua and White (2002) to calculate individual points' loading time in the transverse direction for dual-tyre loading.

Potential Wander Distributions of Automated Vehicles

To study the impact of the AVs' on pavement rutting, we assumed two possible wander distributions for AVs, naming the 'zero-wander' and 'uniform-wander'. In the case of zero-wander, the AVs have no lateral movement. In this case, a constant loading time of 237720 seconds was applied simultaneously on two rectangular areas regardless of the lane width. Figure 3 shows the zero loading time distribution of the AVs. It should be noted that the zero-wander case is a hypothetical situation, and there is always a bit of wander due to wind load and other possible factors, which are excluded in this study.

The other possible wheel wander distribution for AVs is a uniform-wander distribution. In this case, AVs can use the road lane's available width, which is derived by subtracting the truck's width from the lane width. Benefiting from the AVs' programmable capability, the vehicle's lateral wandering pattern is programmed so that the tyre's loading time would be a constant number in all the transverse points within the loading spans. The overall width of a standard 18-wheel truck is around 2.59 m (8.5 ft.). Hence, the remaining space for the truck's lateral wandering for lane widths of 3.5 m, 3.25 m, and 3 m are 0.91 m, 0.66 m, and 0.41 m, respectively. The loading span is extended by 0.1 m from each side to consider the difference between the overall truck width and the out-to-out axle track width, providing more space for wheel wandering (Harwood *et al.*, 2003).

For Peer Review Only

Therefore, the loading spans for lane widths of 3.5 m, 3.25 m, and 3 m, are 1.11 m, 0.86 m, and 0.61 m, respectively (i.e., the boundary values with reference to the centre of the dual tyre ($x = 0$) are -0.55 to 0.55, -0.43 to 0.43, and -0.3 to 0.3, respectively).

To calculate the uniform-wander distribution in this study, we uniformly distributed the total loading through the determined loading spans so that each transverse point receives equal loading time. This uniform loading time could be calculated by dividing the total loading scheme area by each lane width's loading span. The no-wander condition's total loading time should first be calculated to determine the total loading scheme area. In the no-wander case, the total loading time of 237720 seconds is applied simultaneously on two rectangular areas with a width of 0.193 m. In this case, the total loading scheme area would be $91759.92\ ms$ (*i.e.*, $237720 \times 2\ \times 0.193$). The uniform loading time can be driven by dividing the total loading scheme area by the loading spans for each lane width. Therefore, the uniform loading time for lane widths of 3.5 m, 3.25 m, and 3 m are 83188.21 s, 107568.13 s, and 152162.24 s, respectively. Figure 4 shows the uniform loading time distributions of AVs for 30 million passes.

[Figure 2 near here]

[Figure 3 near here]

[Figure 4 near here]

Evaluation Scenarios

There is as yet no consensus on how AVs and HDVs will interact in the future, and the consequences of using either the same travel lanes or separate lanes for AVs are currently under intensive investigation (Liu and Song, 2019; Mohajerpoor and Ramezani, 2019; Amirgholy, Shahabi and Oliver Gao, 2020; Razmi Rad *et al.*, 2020). The focus of this study is on the case in which AVs use a dedicated lane. To assess the effects of allocating narrower lanes for AVs, this

For Peer Review Only

paper considers two alternative scenarios. In the first scenario, the dedicated lane for AVs is narrower than the lanes dedicated for HDVs, and in the second one, the lanes dedicated for AVs and HDVs have the same lane widths. Six sub-scenarios are considered in each scenario to study the effects of lane widths and wander distribution. In total, 12 scenarios are considered and presented in Table 2.

[Table 2 near here]

Results

The loading time distributions shown in Figures 2-4 were imported into the FE model to calculate the rutting depths. The pavement rutting simulation for one dual tyre after 30 million passes of vehicles at a speed of 90 km/h was performed, and the creep strain (CE) values of the pavement structure were determined. Figures 5-7 show the deformed profiles of the asphalt layer as well as the CE values under a dual tyre loading with normal-, zero-, and uniform-wander distributions, respectively, and for each lane width classification. In the classical FE method, the permanent displacement is not considered as a degree of freedom at the element's nodes and, therefore, it is not possible to calculate the rutting depths directly from the FE model (Abu Al-Rub *et al.*, 2012). However, it can be calculated numerically by dividing the pavement's thickness into several sub-layers and integrating the magnitude of the sub-layers' viscoplastic deformation. Accordingly, each transverse point's rutting depth can be determined by the summation of the accumulated CE in the sublayers multiplied by the associated thicknesses. The calculated maximum compressive rutting, maximum uplift rutting, and the total rutting depth in the abovementioned evaluation scenarios are presented in Table 3. As shown in this table, for the HDVs' lane, the normal-wander mode is used, and the total rutting depths for the lane widths of 3 m, 3.25 m, and 3.5m are 1.4 mm, 1.05 mm, and 0.77 mm, respectively. In the same order, using a

For Peer Review Only

uniform distribution for AVs, we observed the total rutting depth of 12.53 mm, 11.16 mm, and 10.4 mm, while in the case of zero-wander distribution for AVs, the total rutting depth is independent of lane width and equals to 18.04 mm.

Figure 8 illustrates the rutting depth profile of the deformed pavement under normal-wander mode for each lane width. As shown in this figure, the maximum compressive rutting is observed in the centre of the pavement transverse profile. It can be seen that when the lane width increases, the total rutting depth decreases. For example, the total rutting depth for 3.5 m lane width is 45% less than 3m.

Considering the lanes dedicated for AVs, the rutting depth profiles with zero- and uniform-wander distributions are shown in Figure 9. A comparison between the zero- and uniform-wander distributions for AVs revealed that in the case of a uniform distribution, the observed total rutting depth would be 42.35%, 38.14%, and 30.54% lower than the zero-wander cases for the lane widths of 3 m, 3.25 m and 3.5 m, respectively.

Considering the evaluation scenarios and corresponding rutting depths mentioned in Table 3**,** the minimum rutting depth for the HDVs' lane is observed at the lane width of 3.5 m. For the lanes dedicated to AVs, the minimum rutting value has occurred when using a uniform-wander distribution and also in the lane width of 3.5 m. Accordingly, scenario 2b would result in the minimum rutting depth for both AVs' and HDVs' lanes compared to the other scenarios.

To compare the pavement performance of the HDVs' and AVs' lanes, the rutting profiles of the deformed pavement under normal-, uniform-, and zero-wander distributions are illustrated in Figures 10-12 for each lane width classification. As can be seen in these figures, AVs with zero-wander distribution in all lane width classifications yield the highest total rutting depth. Given the lane widths of 3 m, 3.25 m, and 3.5 m, the total rutting depth of the zero-wander cases is 12.88,

For Peer Review Only

17.18, and 27.75 times bigger than the one in the normal distribution, and it is also 1.73, 1.62, and 1.44 times bigger than the one in the uniform distribution.

As can be observed, in the case of a uniform-wander distribution, the maximum compressive rutting depth occurs at a point near the edge of the loading area. Although the uniform-wander distribution allows AVs to distribute the load uniformly in the lane's entire available space, the total rutting depths are higher when compared to the normal-wander case.

[Figure 5 near here]

[Figure 6 near here]

[Figure 7 near here]

[Table 3 near here]

[Figure 8 near here]

[Figure 9 near here]

[Figure 10 near here]

[Figure 11 near here]

[Figure 12 near here]

Discussion

As previously mentioned, the present understanding of AVs lateral wandering and its effects on pavement rutting performance is limited and is still relatively undeveloped. However, the results presented here confirmed the current consensus of the previous studies (Chen, Balieu and Kringos, 2016; Noorvand and Underwood, 2017; Chen *et al.*, 2019; Zhou *et al.*, 2019) that automatic wheel wander control of AVs could significantly influence the pavement long-term rutting performance and the way of influencing depends on AVs' wander distribution modes. The primary possible wander distribution mode of AVs, which have been investigated in some of the

For Peer Review Only

previous studies (Chen, Balieu and Kringos, 2016; Noorvand and Underwood, 2017; Chen *et al.*, 2019), is zero-wander distribution mode, which stems from AVs' potential ability of lane centring and keeping a fixed lateral distance from the road edge. This zero-wander distribution results in channelized traffic with no lateral wandering (except a very negligible wander due to potential wind load) and would concentrate the tyre loading area on a specific wheel track in the lane and could accelerate pavement damage and reduce the pavement rutting performance (Chen, Balieu and Kringos, 2016; Noorvand and Underwood, 2017; Chen *et al.*, 2019). The simulation results of our study also provide conclusive support for this finding. As it is discussed above, using the zero-wander distribution for AVs in the future would significantly decrease the pavement lifespan when compared with that in the case of HDVs with normal-wander distribution. Nevertheless, since the zero-wander distribution is not affected by lane width, using narrower lanes for AVs with no lateral wandering could save space and construction and maintenance costs without additional negative impact on pavement performance compared to the wider lanes. So, the question raised by this study necessitates further investigations and highlights the importance of analysing the costs of increased pavement rutting depth induced from zero-wander distribution and the benefits of saving construction and maintenance costs caused by using narrower lanes for AVs.

Since AVs are equipped with more accurate steering control systems compared with HDVs, it is possible to design different lateral wandering patterns for AVs in the future. Accordingly, some of the previous studies (Noorvand and Underwood, 2017; Chen *et al.*, 2019; Zhou *et al.*, 2019) suggested uniform-wander distribution as a more optimized lateral wandering pattern for AVs, which could cover more space of the available lane width and improve pavement rutting performance when compared to the HDVs case. However, the results observed in our study do not support this view. Our study's most striking finding is that by using the uniform-wander

For Peer Review Only

distribution for AVs, the maximum rutting depth would increase significantly compared to the normal distribution for HDVs. As shown in figures 10, 11, and 12, for the uniform-wander mode, the maximum total rutting depth was observed in the edge points of the loading scheme, where there is an abrupt change in the loading time (i.e., the loading time starts immediately at its maximum value). From a mechanical point of view, once the loading process begins, the abrupt change of loading on the loading area edges starts to form two peak points (i.e., maximum compressive rutting and maximum uplift rutting) on both sides of the edges of the loading scheme. By continuing the loading process, the positions of these peak rutting points remain almost fixed (unlike the normal-mode). However, the magnitude of the rutting depth in both peak points accumulates. Therefore, this accumulated rutting at the peak points causes a significant total rutting depth at the loading scheme's edges.

On the contrary, and in normal-wander mode, there is a gradual change in the loading time from the side points. By carefully reviewing the FE model's rutting simulation process for the normal-wander mode, we observed that the maximum total rutting depth was primarily formed at the side points at the beginning of the loading process. By continuing the loading process, the new vehicle passes compensate the existing peak rutting depths at the side points and gradually move the peak rutting point toward the centre. In other words, in the normal distribution case, the maximum rutting depth is not accumulated in a fixed peak point (like the uniform-wander) but is compensated in the side points and is eventually formed at the centre point. In this way, the total rutting depth's magnitude remains almost constant after a certain number of vehicle passes.

Accordingly, the discrepancy between our study's results and the previous studies (Noorvand and Underwood, 2017; Chen *et al.*, 2019; Zhou *et al.*, 2019) in terms of uniform-wander distribution effects can be explained by the observed critical deformation points. In our study,

For Peer Review Only

although the rutting depth observed in the centre point of the rutting profile is not significant for the uniform-wander, the maximum deformation of the asphalt layer occurred near the edges of the loading scheme (see Figures 10-12). It is noteworthy that the measurement points are not distinctly mentioned in the results of the studies mentioned above (i.e., Noorvand and Underwood, 2017; Chen *et al.*, 2019; Zhou *et al.*, 2019).

Another reason for the disagreement between the results may be due to differences in analysis methods and assumptions. Noorvand and Underwood (2017) and Zhou et al. (2019) used the MEPDG approach (McCullah and Gray, 2005) to analyse the impacts of uniform-wander distribution of AVs on pavement rutting performance while we used the FE method in our study, which has different assumptions and inputs. Although Chen et al. (2019) also used the FE method to investigate the uniform-wander distribution effects, the difference between their conclusion and our findings might be originated from the different analysis approaches. Chen et al. (2019) used a theoretical approach to calculate a normal-wander distribution for HDVs and a uniform-wander distribution for AVs; however, we used empirical field data to determine the standard deviations (σ) of normal-wander distribution of HDVs. In our view, using empirical field data is closer to reality and will lead to more accurate results compared to a theoretical framework. In this sense, an important point to consider is that the empirical data used in our study also observed cases that override the lane markings, which cause a considerable difference when compared with the theoretical view.

Another finding of this study, which has not been investigated in previous studies, is that using narrower lanes for AVs could significantly increase the uniform-wander distribution's negative impact on pavement rutting performance. Thus, to use narrower lanes and uniform-wander distribution for AVs in the future, it is crucial to analyse the increased rutting depth costs.

For Peer Review Only

Nevertheless, it should be emphasized that our study's findings are consistent with the argument that using uniform-wander distribution in all cases is more appropriate than using the zero-wander distribution for AVs concerning the pavement rutting performance.

The points discussed above necessitate further investigations on AVs' lateral wandering patterns as well as the lane width effect. Since AVs could provide the opportunity to program self-controlled lateral wandering patterns, the challenge for future studies will be the design of more optimized wander distributions to improve the pavement's long-term rutting performance. This study only investigated two lateral wandering patterns for AVs, including zero- and uniform-wander distribution, which both resulted in considerably more rutting depth when compared with the normal distribution in the case of HDVs. This highlights the importance of examining other possible wander distribution modes for AVs along with considering lane width effect to achieve more favourable consequences of AVs deployment in connection with pavement rutting performance. Moreover, taking into account the fact that AVs' steering control system is more accurate than HDVs, it is a point of discussion whether there is a need to consider a safety margin from the road markings for AVs or not. Further investigation needs to be conducted to study the necessity of considering AVs' safety distance and its effects on different aspects of the transportation system and operations. This has significant practical implications meaning that extremely narrow lane widths might not be considered by road designers, given the adverse effects that this could bring about as a result of incorporating the safety distance in the AVs' manoeuvring programmes. Moreover, it is also recommended to design the APT facility to consider the AVs' possible lateral wandering patterns to verify the results of the finite element models of AVs' rutting performance.

For Peer Review Only

In the present study, a dedicated lane for AVs with different lane width scenarios was investigated. Since it is possible to have shared lanes in the near future (i.e., mixed traffic) for AVs and HDVs, it is also necessary to study the mixed traffic impacts together with lane width effect on pavement long-term rutting performance.

This study considered a single pavement structure, pavement materials, tyre pressure, and vehicle characteristic. As the factors mentioned above have the potential to influence the simulation results presented in this study, future research worth also exploring different pavement structures (e.g., thinner asphalt layer), different asphalt mixtures and consider the potential differences between the vehicle characteristics of AVs and HDVs such as vehicle speed profile. Furthermore, in addition to the pavement rutting performance, examining other pavement deterioration modes such as fatigue performance is also desirable.

Conclusions

Based on the simulation results of this study, the following conclusions can be drawn:

- The finite element approach taken in this study shows its merits and provided us with a better insight into the impacts of different loading distribution modes on pavement performance. It is essential to mention that the maximum rutting position is different for different loading schemes (i.e., for the normal distribution, it occurs at the centre, while for the zero- and uniform-wander distributions, it occurs at the load edges).
- The implication of automated vehicles with a uniform- or zero-wander distribution in a dedicated lane would significantly accelerate pavement rutting damage. Considering a lane width of 3.5 m, using a uniform-wander distribution for AVs would result in a 14.49 times larger rutting depth than the case of HDVs. This value would be 27.75 times larger when using a zero-wander distribution for AVs.

For Peer Review Only

- Dedicating a narrower lane for AVs could significantly influence the flexible pavement's rutting performance when a uniform-wander distribution is used for AVs. Using dedicated lane widths of 3 m and 3.25 m for AVs with uniform-wander distribution would increase the total rutting depth of the pavement by 20.48% and 7.31%, respectively, compared to the lane width of 3.5 m. However, in zero-wander distribution for AVs, the total rutting depth is independent of the lane width.
- Using a uniform-wander distribution for AVs could considerably decrease the total rutting depth by 42.35%, 38.13%, and 30.54% compared to the zero-wander distribution mode, given lane widths of 3.5 m, 3.25 m, and 3 m, respectively.

Declaration interest

Declarations of interest: none

For Peer Review Only

References

Abu Al-Rub, R. K. *et al.* (2012) 'Comparing finite element and constitutive modelling techniques for predicting rutting of asphalt pavements', *International Journal of Pavement Engineering*, 13(4), pp. 322–338. doi: 10.1080/10298436.2011.566613.

Al-Qadi, I. L. *et al.* (2009) 'Creep behavior of hot-mix asphalt due to heavy vehicular tire loading', *Journal of Engineering Mechanics*, 135(11), pp. 1265–1273. doi: 10.1061/(ASCE)0733-9399(2009)135:11(1265).

Amirgholy, M., Shahabi, M. and Oliver Gao, H. (2020) 'Traffic automation and lane management for communicant, autonomous, and human-driven vehicles', *Transportation Research Part C: Emerging Technologies*. Elsevier, 111(November 2019), pp. 477–495. doi: 10.1016/j.trc.2019.12.009.

Benekohal, R. F., Hall, K. T. and Miller Harlan w (1958) 'Effect of Lane Widening on Lateral Distribution of Truck Wheels', *Transportation Research Record*, (14), pp. 57–66.

Blab, R. and Litzjw, J. (1995) 'Measurements Of The Lateral Distribution Of Heavy Vehicles And Its Effects On The Design Of Road Pavements', in *International Symposium on Heavy Vehicle Weights and Dimensions*, pp. 389–396.

Buiter, R. *et al.* (1989) 'Effects of transverse distribution of heavy vehicles on thickness design of full-depth asphalt pavements', *Transportation Research Record*, (1227), pp. 66–74.

Charles, D. and Cas, J. (2017) 'Mobility • Safety • Economy • Environment Readiness of the road network for connected and autonomous vehicles', (April). Available at: www.racfoundation.org.

Chen, F. *et al.* (2019) 'Assess the impacts of different autonomous trucks' lateral control modes on asphalt pavement performance', *Transportation Research Part C: Emerging Technologies*. Elsevier, 103(March), pp. 17–29. doi: 10.1016/j.trc.2019.04.001.

For Peer Review Only

Chen, F., Balieu, R. and Kringos, N. (2016) 'Potential Influences on Long-Term Service Performance of Road Infrastructure by Automated Vehicles', *Transportation Research Record: Journal of the Transportation Research Board*, 2550(1), pp. 72–79. doi: 10.3141/2550-10.

Dennis, E. P. *et al.* (2017) 'Planning for Connected and Automated Vehicles', (March), pp. 1–37.

Erlingsson, S. (2004) 'Mechanistic Pavement Design Methods – A Road to Better Understanding of Pavement Performance', *Via Nordica 2004 – NRA's 19th Road Congress, C8: Berekraftige vegkonstruksjonar*, (June 2014), pp. 1–8. Available at: https://www.researchgate.net/publication/242219834_Mechanistic_Pavement_Design_Methods_-_A_Road_to_Better_Understanding_of_Pavement_Performance.

Erlingsson, S., Said, S. and McGarvey, T. (2012) 'Influence of Heavy Traffic Lateral Wander on Pavement Distribution', *In EPAM-4th European Pavement and Asset Management conference. Statens väg-och transportforskningsinstitut*.

Fagnant, D. J. and Kockelman, K. (2015) 'Preparing a nation for autonomous vehicles: Opportunities, barriers and policy recommendations', *Transportation Research Part A: Policy and Practice*. Elsevier Ltd, 77, pp. 167–181. doi: 10.1016/j.tra.2015.04.003.

Fang, H. *et al.* (2007) 'An object-oriented framework for finite element pavement analysis', *Advances in Engineering Software*, 38(11–12), pp. 763–771. doi: 10.1016/j.advengsoft.2006.08.045.

Gungor, O. E. and Al-Qadi, I. L. (2020) 'All for one: Centralized optimization of truck platoons to improve roadway infrastructure sustainability', *Transportation Research Part C: Emerging Technologies*. Elsevier, 114(February), pp. 84–98. doi: 10.1016/j.trc.2020.02.002.

Harwood, D. W. *et al.* (2003) *Review of Truck Characteristics as Factors in Roadway Design*, *Review of Truck Characteristics as Factors in Roadway Design*. doi: 10.17226/23379.

For Peer Review Only

HCM 2010 : highway capacity manual (2010). Fifth edition. Washington, D.C. : Transportation Research Board, c2010-.

Hua, J. (1998) *Finite element modeling and analysis of accelerated pavement testing device and rutting phenomenon*.

Hua, J. and White, T. (2002) 'A Study of Nonlinear Tire Contact Pressure Effects on HMA Rutting', *The International Journal of Geomechanics*, 2(May 2001), p. 45. doi: 10.1061/(ASCE)1532-3641(2002)2.

Huang, H. (1995) *Analysis of accelerated pavement tests and finite element modeling of rutting phenomenon*. Purdue University by Haiming Huang.

Johnson, C. (2017) 'Readiness of the road network for connected and autonomous vehicles', *RAC Foundation*, (April), pp. 1–42.

Kockelman, K. *et al.* (2016) 'An assessment of autonomous vehicles: Traffic impacts and infrastructure needs. Final Report', *Center for Transportation Research the University of Texas at Austin*, p. 182. doi: 10.1016/j.profnurs.2009.01.003.

Lee, C. E. and Shankar, P. R. (1983) 'Lateral Placement of Trucks in Highway Lanes', (3).

Litman, T. A. (2015) 'Autonomous Vehicle Implementation Predictions Implications for Transport Planning', *Traffic Technology International*, pp. 36–42. Available at: www.vtpi.orgInfo@vtpi.org.

Liu, Z. and Song, Z. (2019) 'Strategic planning of dedicated autonomous vehicle lanes and autonomous vehicle/toll lanes in transportation networks', *Transportation Research Part C: Emerging Technologies*. Elsevier, 106(March), pp. 381–403. doi: 10.1016/j.trc.2019.07.022.

M, S. (2009) 'ABAQUS/Standard User's Manual, Version 6.9.'

McCullah, J. and Gray, D. (2005) *Cooperative Highway Program*.

For Peer Review Only

Mohajerpoor, R. and Ramezani, M. (2019) 'Mixed flow of autonomous and human-driven vehicles: Analytical headway modeling and optimal lane management', *Transportation Research Part C: Emerging Technologies*. Elsevier, 109(November), pp. 194–210. doi: 10.1016/j.trc.2019.10.009.

Noorvand, H. and Underwood, B. S. (2017) 'Hossein Noorvand, B. Shane Underwood, Arizona State University, Tempe, AZ 85287, USA', *Transportation Research Record*, 2640, pp. 21–28. doi: 10.3141/2640-03.

Perl, M., Uzan, J. and Sides, A. (1983) 'Visco-Elasto-Plastic Consititutive Law for a Bituminous Mixture Under Repeated Loading.', *Transportation Research Record*, 47(I), pp. 20–27.

Razmi Rad, S. *et al.* (2020) 'Design and operation of dedicated lanes for connected and automated vehicles on motorways: A conceptual framework and research agenda', *Transportation Research Part C: Emerging Technologies*. Elsevier, 117(October 2019), p. 102664. doi: 10.1016/j.trc.2020.102664.

Timm, D. and Priest, A. (2005) 'Measurement of Wheel Wander Under Live Traffic Conditions', *7th International Conference on the Bearing Capacity of Roads, Railways and Airfields (BCRA'05)*.

Vahidi, A. and Sciarretta, A. (2018) 'Energy saving potentials of connected and automated vehicles', *Transportation Research Part C: Emerging Technologies*. Elsevier, 95(April 2018), pp. 822–843. doi: 10.1016/j.trc.2018.09.001.

White, T. D. *et al.* (2002) *Contributions of Pavement Structural Layers to Rutting of Hot Mix Asphalt Pavements, NCHRP Report 468*, *Transportation Research Board and American Association of State Highway and Transportation Officials*.

Zhou, F. *et al.* (2019) 'Optimization of Lateral Wandering of Automated Vehicles to Reduce

For Peer Review Only

Hydroplaning Potential and to Improve Pavement Life', *Transportation Research Record*, pp. 1–9. doi: 10.1177/0361198119853560.

For Peer Review Only

Table 1. Comparison between the FE model and the APT

Rutting mode	The model results	The APT results	Results ratio
Maximum compressive rutting (m)	0.001478	0.001473	1.00339
Maximum uplift rutting (m)	0.001661	0.001701	0.976

For Peer Review Only

Table 2. Evaluation scenarios

Scenarios		Lane width (m)		Wander distribution	
		Non-AVs	AVs	Non-AVs	AVs
Scenario 1 (Narrower Lane for AVs)	1a	3.5	3.25	Normal	Zero
	1b	3.5	3.25	Normal	Uniform
	1c	3.5	3	Normal	Zero
	1d	3.5	3	Normal	Uniform
	1e	3.25	3	Normal	Zero
	1f	3.25	3	Normal	Uniform
Scenario 2 (Same Lane Width for AVs)	2a	3.5	3.5	Normal	Zero
	2b	3.5	3.5	Normal	Uniform
	2c	3.25	3.25	Normal	Zero
	2d	3.25	3.25	Normal	Uniform
	2e	3	3	Normal	Zero
	2f	3	3	Normal	Uniform

For Peer Review Only

Table 3. Maximum rutting depths in different scenarios

Scenarios		Non-AVs' lane *				AVs' Lane				
		Lane width (m)	Rutting (mm)			Lane width (m)	Distribution	Rutting (mm)		
			Compressive	Uplift	Total			Compressive	Uplift	Total
Scenario1	1a	3.5	0.53	0.24	0.77	3.25	Zero	9.87	11	18.04**
	1b	3.5	0.53	0.24	0.77	3.25	Uniform	6.37	4.79	11.16
	1c	3.5	0.53	0.24	0.77	3	Zero	9.87	11	18.04
	1d	3.5	0.53	0.24	0.77	3	Uniform	7.32	5.21	12.53
	1e	3.25	0.6	0.45	1.05	3	Zero	9.87	11	18.04
	1f	3.25	0.6	0.45	1.05	3	Uniform	7.32	5.21	12.53
Scenario2	2a	3.5	0.53	0.24	0.77	3.5	Zero	9.87	11	18.04
	2b	3.5	0.53	0.24	0.77	3.5	Uniform	5.82	4.58	10.4
	2c	3.25	0.6	0.45	1.05	3.25	Zero	9.87	11	18.04
	2d	3.25	0.6	0.45	1.05	3.25	Uniform	6.37	4.79	11.16
	2e	3	0.65	0.75	1.4	3	Zero	9.87	11	18.04
	2f	3	0.65	0.75	1.4	3	Uniform	7.32	5.21	12.53

* In all scenarios, non-AVs have normal wander distribution

** Rutting mode type 2

For Peer Review Only

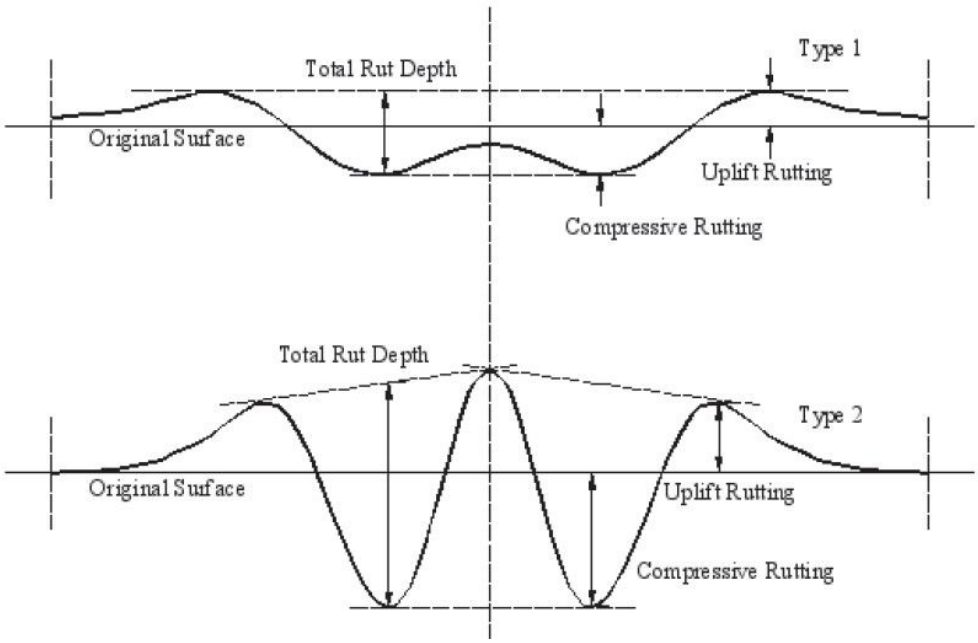

Figure 1. Rutting modes (Hua and White, 2002)

17x11mm (1200 x 1200 DPI)

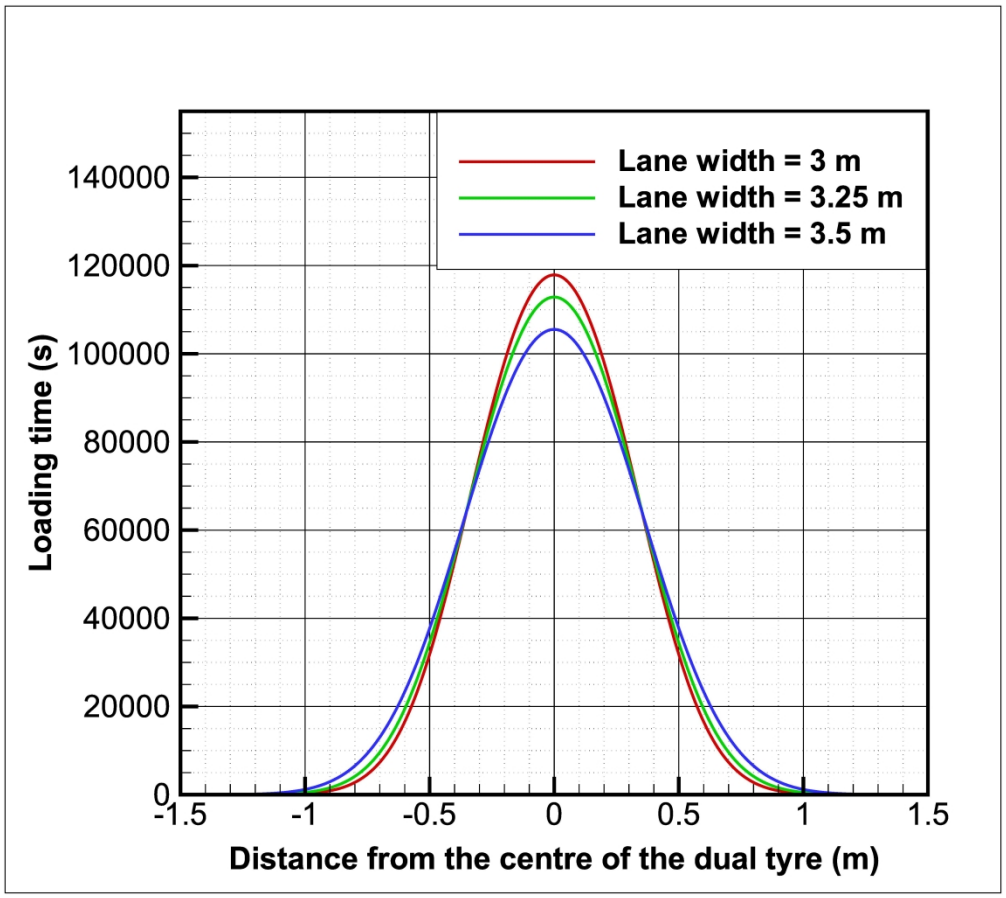

Figure 2. Normal distributions of loading time for HDVs for one dual tyre for each lane width

210x186mm (600 x 600 DPI)

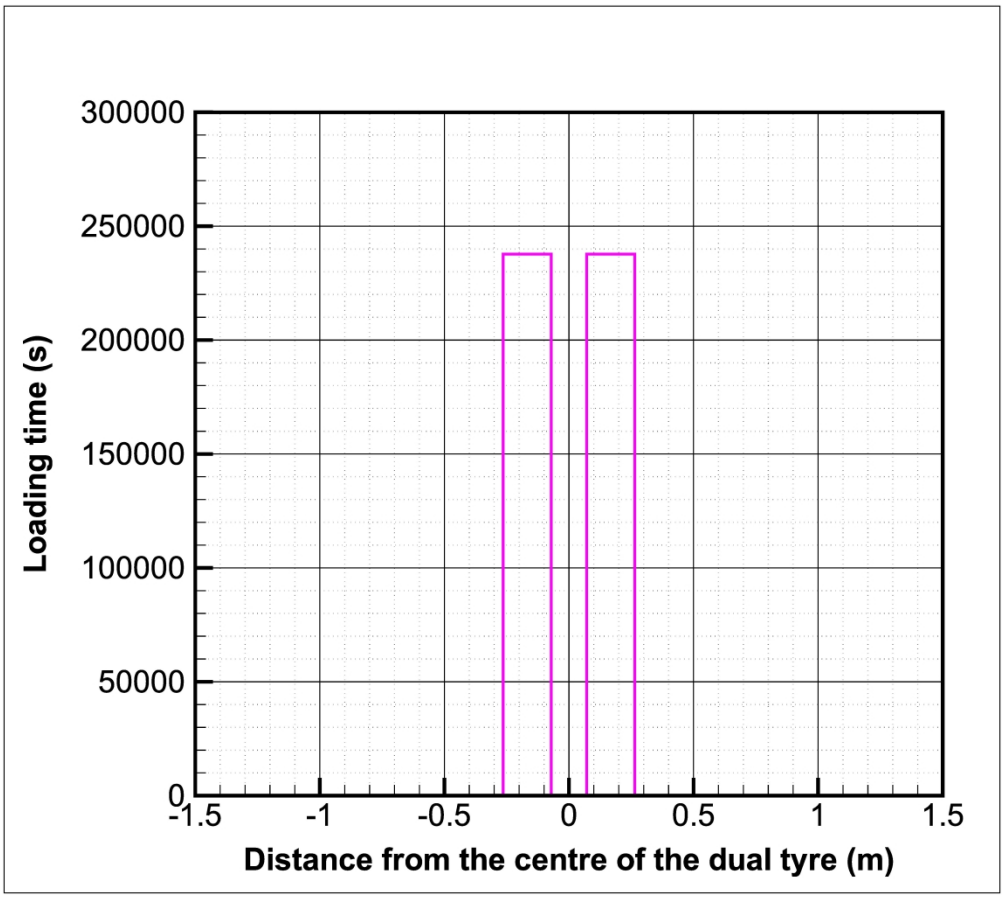

Figure 3. Zero loading time distribution of AVs for one dual tyre

210x186mm (600 x 600 DPI)

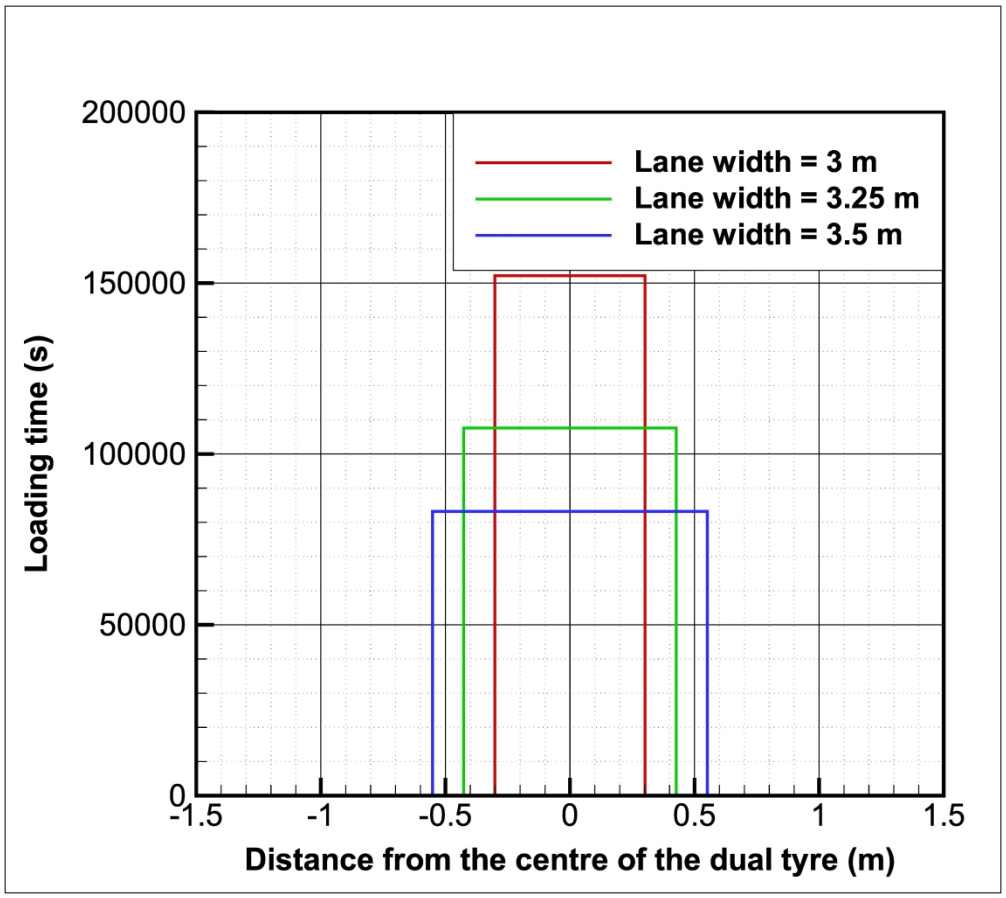

Figure 4. Uniform loading time distribution of AVs for one dual tyre for each lane width

210x186mm (600 x 600 DPI)

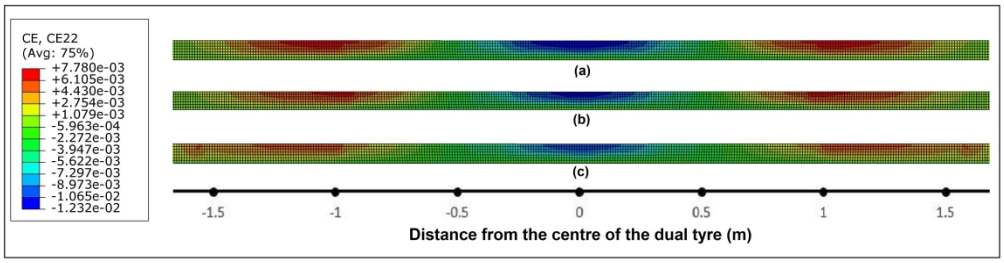

Figure 5. Distributions of accumulated creep strain after 30 million passes of HDVs with normal-wander distribution: (a) lane width of 3 m (b) lane width of 3.25 m (c) lane width of 3.5 m

103x26mm (1200 x 1200 DPI)

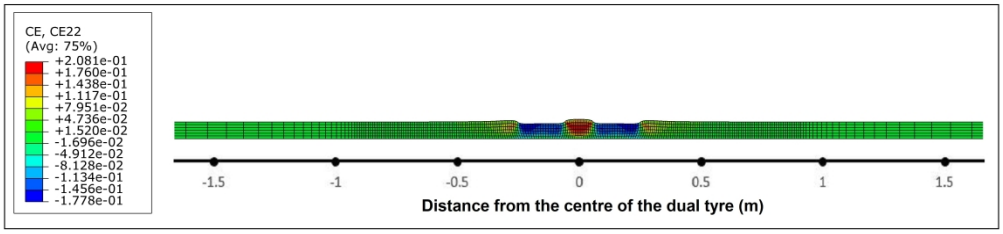

Figure 6. Distributions of accumulated creep strain after 30 million passes of AVs with zero-wander distribution

103x24mm (1200 x 1200 DPI)

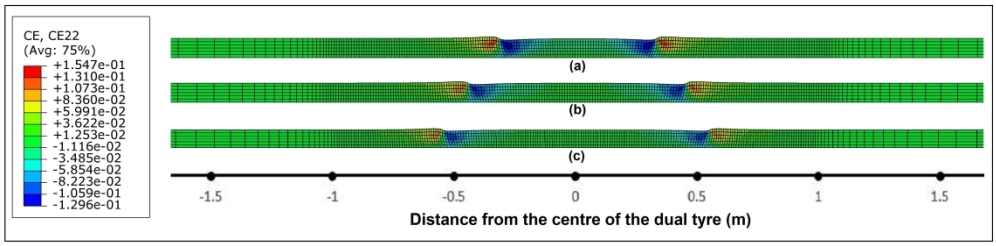

Figure 7. Distributions of accumulated creep strain after 30 million passes with uniform-wander distribution: (a) lane width of 3m (b) lane width of 3.25m (c) lane width of 3.5m

103x25mm (1200 x 1200 DPI)

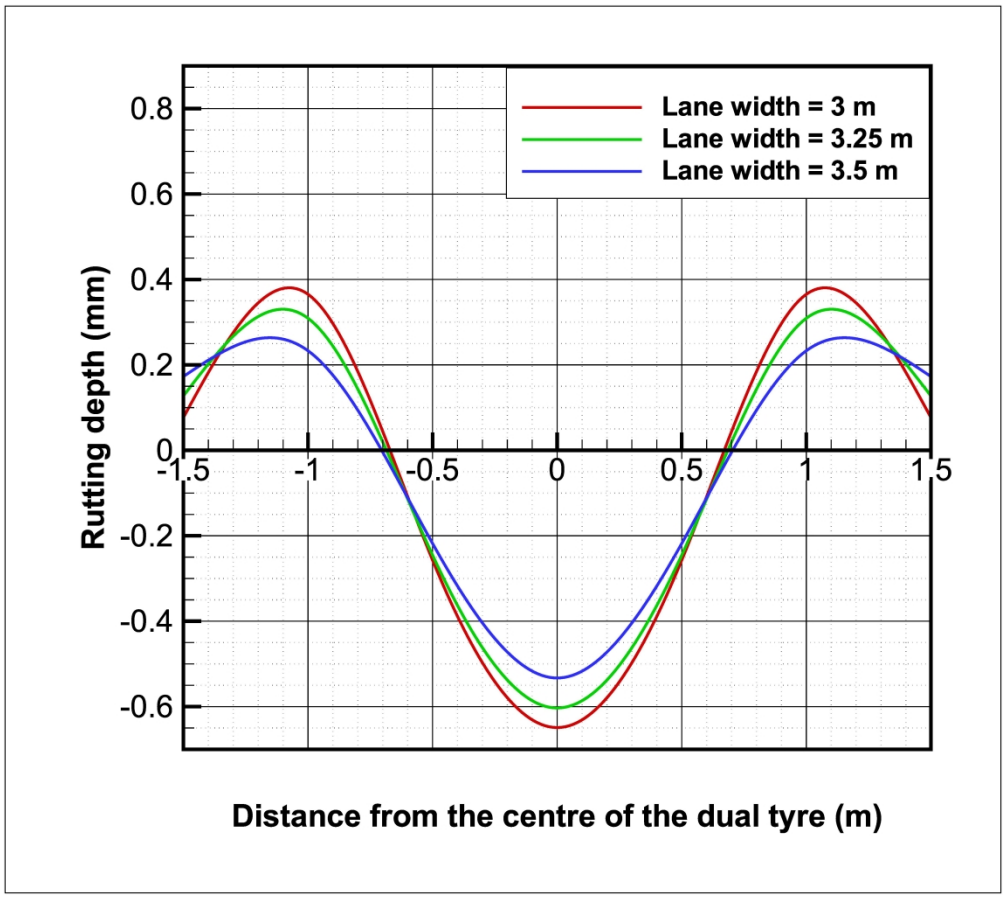

Figure 8. Rutting depth profile of HDVs' lane with normal-wander distribution of one dual tyre for the lane widths of 3.5 m, 3.25 m and 3 m

210x186mm (600 x 600 DPI)

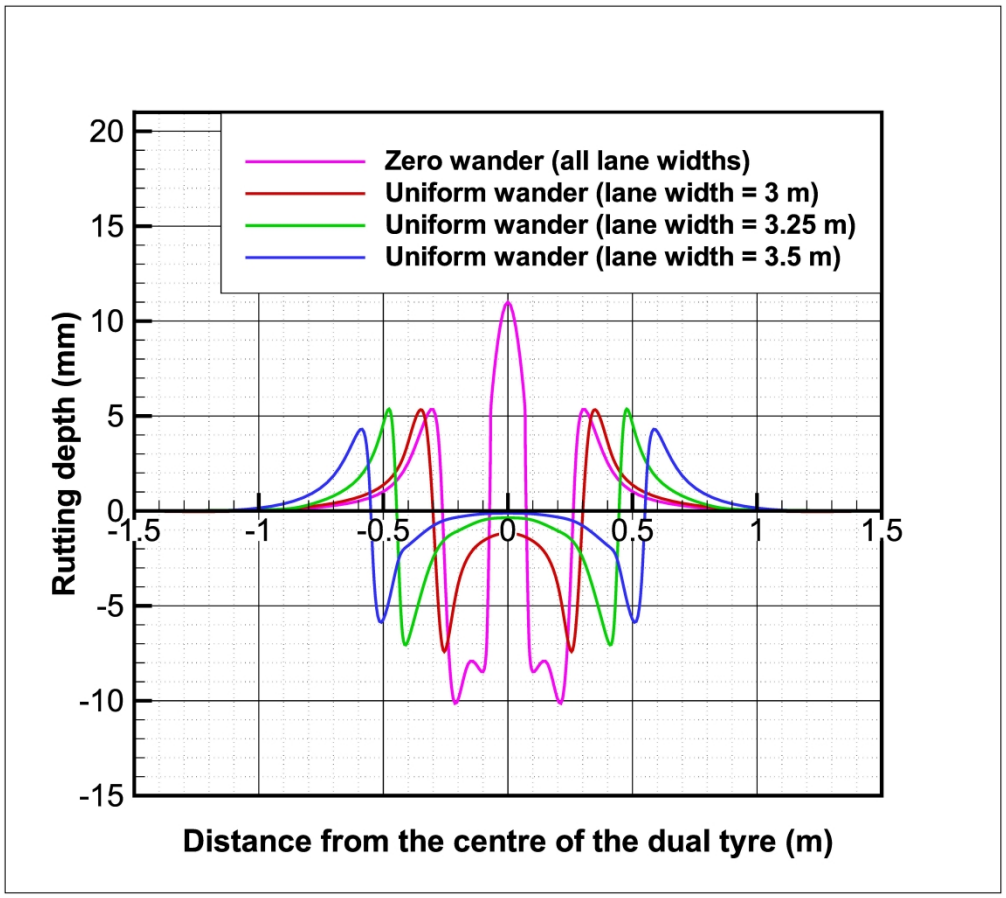

Figure 9. Rutting depth profile of AVs' lane with zero- and uniform-wander distribution of one dual tyre for the lane widths of 3.5 m, 3.25 m and 3 m (zero-wander is independent of lane width)

210x186mm (600 x 600 DPI)

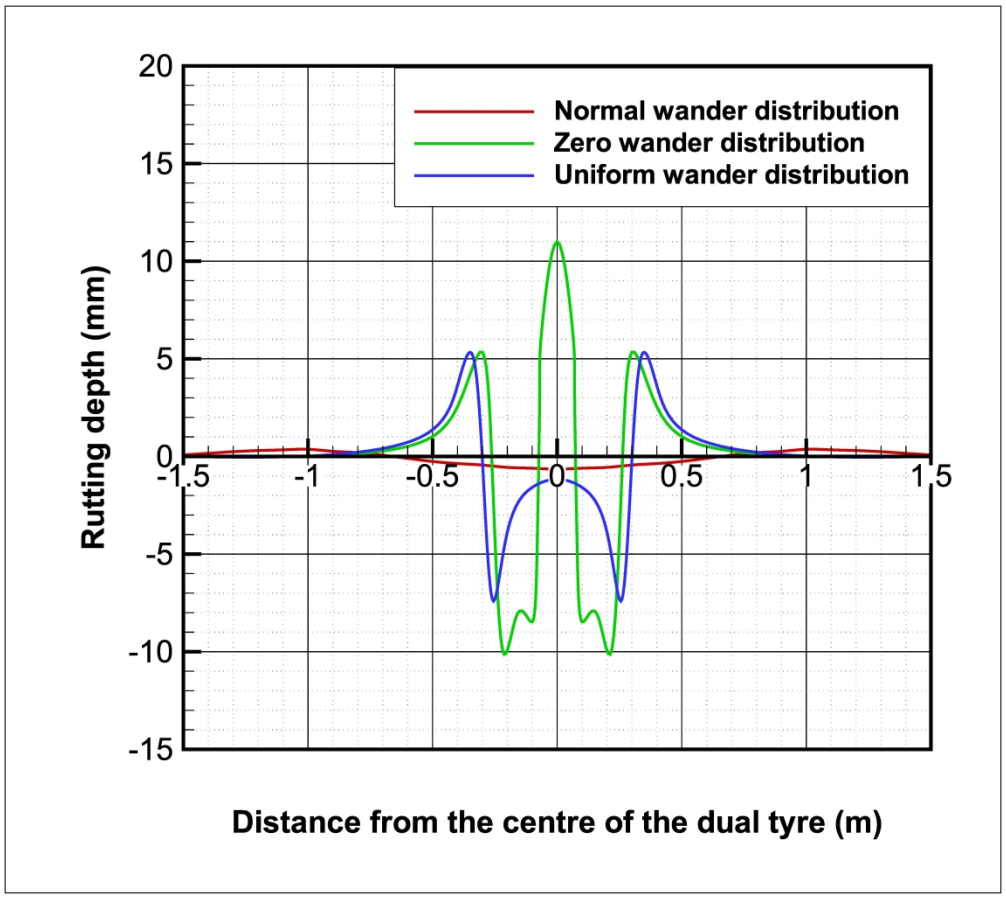

Figure 10. Rutting depth profile of the deformed pavement with normal-, zero-, and uniform-wander mode for lane width of 3 m

210x186mm (600 x 600 DPI)

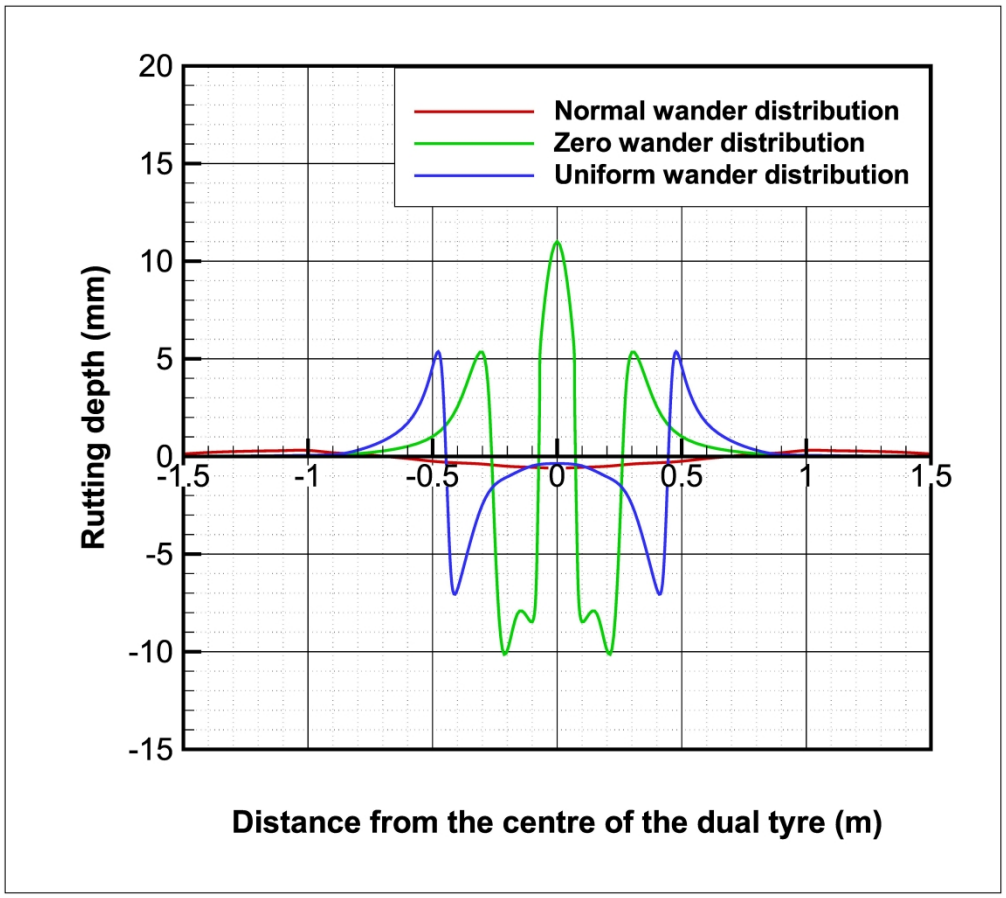

Figure 11. Rutting depth profile of the deformed pavement with normal-, zero-, and uniform-wander mode for lane width of 3.25 m

210x186mm (600 x 600 DPI)

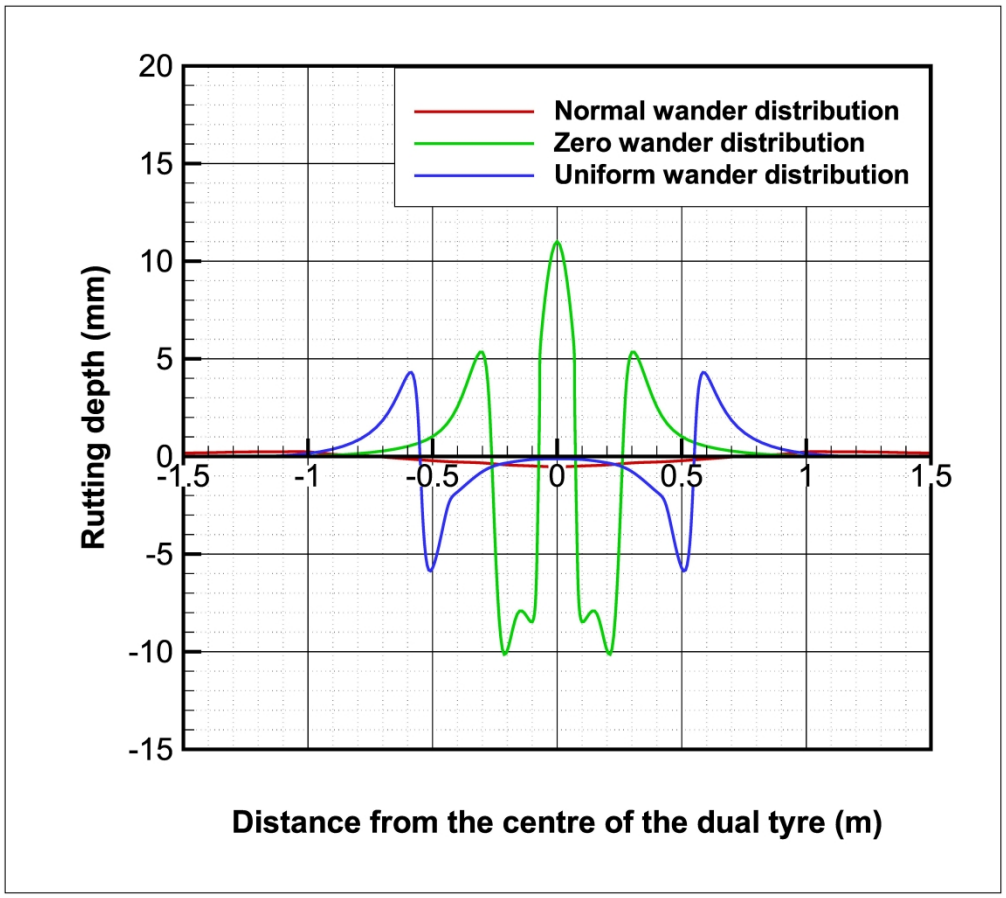

Figure 12. Rutting depth profile of the deformed pavement with normal-, zero-, and uniform-wander mode distribution for lane width of 3.5 m

210x186mm (600 x 600 DPI)